Journal Pre-proof

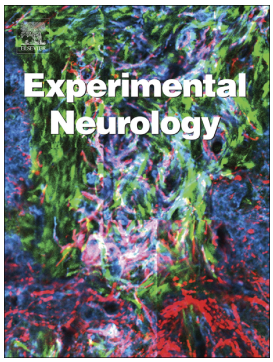

Hippocampal demyelination is associated with increased magnetic susceptibility in a mouse model of concussion

Xuan Vinh To, Viktor Vegh, Naana Owusu-Amoah, Paul Cumming, Fatima A. Nasrallah

PII: S0014-4886(23)00090-0

DOI: https://doi.org/10.1016/j.expneurol.2023.114406

Reference: YEXNR 114406

To appear in: *Experimental Neurology*

Received date: 19 December 2022

Revised date: 4 April 2023

Accepted date: 6 April 2023

Please cite this article as: X.V. To, V. Vegh, N. Owusu-Amoah, et al., Hippocampal demyelination is associated with increased magnetic susceptibility in a mouse model of concussion, *Experimental Neurology* (2023), https://doi.org/10.1016/j.expneurol.2023.114406

Hippocampal Demyelination is Associated with Increased Magnetic Susceptibility in a Mouse Model of Concussion

Xuan Vinh To[1], Viktor Vegh[2,3], Naana Owusu-Amoah[1], Paul Cumming[4,5] and Fatima A. Nasrallah[1,2]*

[1] *The Queensland Brain Institute, The University of Queensland, Australia.*

[2] *The Centre for Advanced Imaging, The University of Queensland, Australia*

[3] *The ARC Centre for Innovation in Biomedical Imaging Technology, Brisbane, Australia*

[4] *Department of Nuclear Medicine, Bern University Hospital, Bern, Switzerland*

[5] *School of Psychology and Counselling, Queensland University of Technology, Brisbane, Australia*

*Corresponding author

Address correspondence to:

Fatima Nasrallah

The Queensland Brain Institute, The University of Queensland

Building 79, Upland Road, Saint Lucia, Brisbane, Queensland, Australia 4072

Phone: +61 7 3346 0322

Fax +61 7 3346 6301

Email: f.nasrallah@uq.edu.au

Abstract

Structural and functional deficits in the hippocampus are a prominent feature of moderate-severe traumatic brain injury (TBI). In this work, we investigated the potential of Quantitative Susceptibility Imaging (QSM) to reveal the temporal changes in myelin integrity in a mouse model of concussion (mild TBI). We employed a cross-sectional design wherein we assigned 43 mice to cohorts undergoing either a concussive impact or a sham procedure, with QSM imaging at day 2, 7, or 14 post-injury, followed by Luxol Fast Blue (LFB) myelin staining to assess the structural integrity of hippocampal white matter (WM). We assessed spatial learning in the mice using the Active Place Avoidance Test (APA), recording their ability to use visual cues to locate and avoid zone-dependent mild electrical shocks. QSM and LFB staining indicated changes in the stratum lacunosum-molecular layer of the hippocampus in the concussion groups, suggesting impairment of this key relay between the entorhinal cortex and the CA1 regions. These imaging and histology findings were consistent with demyelination, namely increased magnetic susceptibility to MR imaging and decreased LFB staining. In the APA test, sham animals showed fewer entries into the shock zone compared to the concussed cohort. Thus, we present radiological, histological, and behavioral findings that concussion can induce significant and alterations in hippocampal integrity and function that evolve over time after the injury.

Keywords: quantitative susceptibility mapping; multi-compartment modelling; concussion

Introduction

Concussion, also known as mild traumatic brain injury (mTBI), is the most common form of TBI, with an estimated incidence of 600 cases/100,000 population per year.[1] While considered a mild injury, many individuals suffer post-concussion symptoms[2,3] that can persist for weeks following the impact, potentially leading to long-term neuroradiological defects and cognitive impairments.[4] Indeed, the outcome of concussion is highly variable with respect to the severity and duration of such symptoms, and presents difficulties in obtaining objective imaging-based endpoints that might guide individual patient management.[5,6]

Routine structural imaging findings in concussion are often unremarkable, although a number of studies have shown subtle changes in the brain.[7] More advanced imaging methods, such as diffusion tensor imaging (DTI) of white matter (WM) integrity have provided more specific information on the sequelae of concussion,[8–14] although results have been contradictory and the patterns of changes are time-dependent.[15] Indeed, previous magnetic resonance imaging (MRI) findings in rodent models of TBI have emphasized the compromised WM integrity in the aftermath of TBI.[16,17] In contrast, our previous studies in a mouse model of concussion[18,19] showed the preponderance of imaging findings after a single impact we present in the grey matter (GM).[18] Quantitative susceptibility mapping (QSM) is another advanced MRI technique, which takes advantage of the magnetic properties of tissue inducing distinct changes in the signal phase, from which the magnetic properties of tissue at the voxel-level are inferred.[20] QSM has been applied in studies of myelin breakdown, myelin debris degradation and removal, and iron accumulation in multiple sclerosis,[21] the demyelination and remyelination process in a cuprizone mouse model,[22,23] and thalamic calcium influx in a repeated mild TBI model.[24] Given the inherent myelin-sensitivity of QSM, we aimed to employ it to test for effects of concussion on myelin integrity in mouse brain. We also undertook histological assessment of myelin staining and tested spatial learning for correlation with the QSM results.

Experimental procedures

Details of study design, concussion procedure, animal handling, structural MRI acquisitions and image processing are as described in our earlier publication;[18] relevant details are mentioned here for the readers' convenience.

Study design and concussion procedure

This is a cross-sectional study which included 43 male mice aged 13.2 ± 1.4 weeks at the time of sham or verum concussion. Mice were divided into four cohorts: Sham at days 2 (n = 6), 7 (n = 3) and 14 (n = 5), and post-concussion (CON) days 2 (n = 9), 7 (n = 10), and 14 (n = 10). On day 0, all CON mice were exposed to a concussive impact using our impactor device (see our earlier study[19] for detailed description). In brief, we anaesthetized the animals with 3% isoflurane in 60% air and 40% O_2, and then restrained them on their backs with Velcro straps across their chest and abdomen, with the rostral restraint just below the axilla. We positioned the body on a non-slip pad at a 45 degrees incline, with the head placed over a hole through which a brass piston could deliver the impact. The sham animals underwent exactly the same procedure, but did not receive an impact.

At days 2, 7, or 14, depending on the cohort, mice underwent behavioral assessment and MRI scanning. No animals met our exclusion criteria of obvious brain injuries or structural abnormalities on T2-weighted MRI, including areas of obvious hyper- or hypo-intensity and tissue loss. All experiments were approved by the Institutional Animal Ethics Committee at the University of Queensland (Animal Ethics Committee approval number QBI/260/17). Data from this study are available upon reasonable request to the corresponding author.

Active Placement Avoidance (APA) test

On the day prior to the MRI scan, the animals were acclimated for two minutes in the APA trial room for habituation to experimenter's handling. Next, we placed the animals in the APA rig for a 10-minutes habituation trial without electric shocks. Long-term memory paradigm for APA trials commonly involve multiple daily trials extending over several days.[25] In this injury model, the animals would have had to acquire and recall spatial memory while undergoing dynamic changes and recovery from the concussion injury, which would confound the interpretation of results. Furthermore, spatial learning is known to induce rsfMRI changes,[26] such that longitudinal results would entail a mixture of learning/memory and injury effects. The APA trial we used in this study is analogous to cognitive/memory clinical tests as applied in concussion patients.[27]

On the day of the MRI scan, some of the mice (n = 7 for the entire sham cohort and n = 5 for each of the three CON cohorts) were tested for short-term memory using a single 30-minutes APA trial, following a published protocol.[25] In brief, we placed four different visual cues on the room walls and adjusted the ambient illumination to 70 lux. The APA arena (a 77 cm

diameter, 32 cm-high transparent circular boundary) rotated counter-clockwise (1 rpm), and the area floor delivered a brief foot shock using a constant current source (500 ms, 60 Hz, 0.5 mA) when the animal was detected to enter a shock zone (60° arc about the centre of the rotating arena). We placed the animals were in the quadrant opposite to the shock zone at the start of the trial. The animals were tracked using Tracker software (Bio-Signal Group, NY, USA), which recorded the number of entries into the shock zone in intervals of five minutes as an index of the APA test performance. After the APA trial, the mice were anesthetized as above for MRI scanning.

MRI experiments

Animal handling

Anesthesia was induced using 3% isoflurane in 60% air and 40% O_2 delivered at 1L/min, with maintenance anesthesia at 2–2.5% during the procedure, which took around 30 min. Each mouse was positioned on an MRI-compatible cradle (Bruker Biospin, Germany) with ear bars and bite bars to reduce head motion. We inserted and fixed an intraperitoneal (i.p.) catheter for delivery of the α2 adrenergic receptor agonist medetomidine (Domitor, Pfizer, USA). For sedation, we administered an i.p. bolus of 0.05 mg/kg medetomidine, with maintenance by continuous infusion at a rate of 0.1 mg/kg/h. Once the animal was inside the MRI scanner, isoflurane was reduced gradually to approximately 0.25%. The total time under anesthesia for each animal was approximately 2.5 hours. At the end of the scanning session, 1.25 mg/kg atipemazole (Antisedan, Pfizer, USA) was given i.p. for medetomidine reversal. The anesthesia protocol was derived from our earlier resting-state functional MRI study in mice.[28]

Structural MRI scans

MRI scans were performed on a 9.4 T MRI scanner (Bruker Biospin, Germany) equipped with a cryogenically cooled transmit and receive coil, controlled by a console running Paravision 6.0.1 (Bruker Biospin, Germany). Structural imaging data was acquired using a 2D T2-weighted (T2w) turbo rapid acquisition with refocused echoes (TurboRARE) sequence with the following parameters: matrix size = 192 × 192, field of view (FOV) = 19.2 × 19.2 mm^2, number of contiguous slices = 52, and slice thickness = 0.3 mm; giving an

effective spatial resolution of 0.1 × 0.1 × 0.3 mm^3, repetition time (TR) = 7200 ms, echo time (TE) = 39 ms, averages = 4, RARE factor = 8, and bandwidth = 54.3478 kHz.

Multi-echo GRE-MRI scans

Multi-echo GRE-MRI (mGRE-MRI) data were acquired using a 3D multi-echo spoiled gradient recalled echo (GRE) sequence with fat saturation, flow saturation, and FOV saturation (FOV saturation boxes covering the head and neck tissues outside the imaging FOV), monopolar readout, and the following parameters: matrix size = 160 × 160 × 160, FOV size = 16 × 16 × 16 mm^3, effectively resulting in a 0.1 mm^3 isotropic spatial resolution, TR = 50 ms, 8 echoes with minTE/ΔTE/maxTE = 2.654/3.247/25.382 ms, flip angle = 13.5, bandwidth 400.641 Hz/px.

Diffusion MRI scans

Diffusion MRI data were acquired using a diffusion-weighted imaging (DWI) spin-echo echo planar imaging (DWI SE-EPI) sequence with the following parameters: matrix size = 96 × 96, FOV = 19.2 × 19.2 mm, 32 slices of 0.25 mm thickness and 0.05 mm slice gap (giving output spatial resolution of 0.2 × 0.2 × 0.3 mm), TR = 4500 ms, TE = 25 ms, averages = 4, 3 b-value shells with b = 600, 1500, and 2000 s/mm2, 33 diffusion weighted directions for each shell, and 2 b = 0 images. A pair of reference b = 0 SE-EPI scans were acquired with opposite phase-encoding directions for EPI distortion correction.

Tissue collection, histology, and microscopy imaging and analysis

Luxol Fast Blue staining and microscopy imaging

After the scan, the mice were sacrificed by transcardial perfusion-fixation with 0.1 M phosphate-buffered saline (PBS) pre-wash followed by 4% formaldehyde in 0.1 M PBS as fixative. The brains were harvested and post-fixed in 4% formaldehyde in 0.1 M PBS for 16 hours at 4 ^{o}C. The brains were then rinsed with 0.1 M PBS and stored in 0.05% sodium azide in PBS 4 ^{o}C until further processing. Approximately three brains from each of four groups (CON day 2, CON day 7, CON day 14 and sham) were selected randomly for further processing. The selected brains were embedded in paraffin and cut into 10 μm-thick coronal sections on a microtome (Leica semi-automated RM2245 rotary microtome). Every 30th section was dewaxed, washed, and stained using the Luxol fast blue (LFP) stain. The stained

sections were coversliped with DPX mounting media and imaged using a brightfield slide scanner (Metafer Vslide Scanner by MetaSystems, Germany, driven by Zeiss Axio Imager Z2) at 20× magnification. Microscopy images were exported as 32-bit RGB OME-TIFF images for further analysis.

Histology image processing and analysis

Further image processing and analysis were performed using the FIJI software[29] (ImageJ2 v. 1.53c). Slide scanner images were cropped to individual sections and the LFP RGB images were converted to CIELAB color space[30] L*a*b* stacks, and the a* images were selected for providing the clearest contrast between myelin-rich and myelin-poor regions (Figure 1A). The a* images were median filtered using an 8 µm radius kernel.

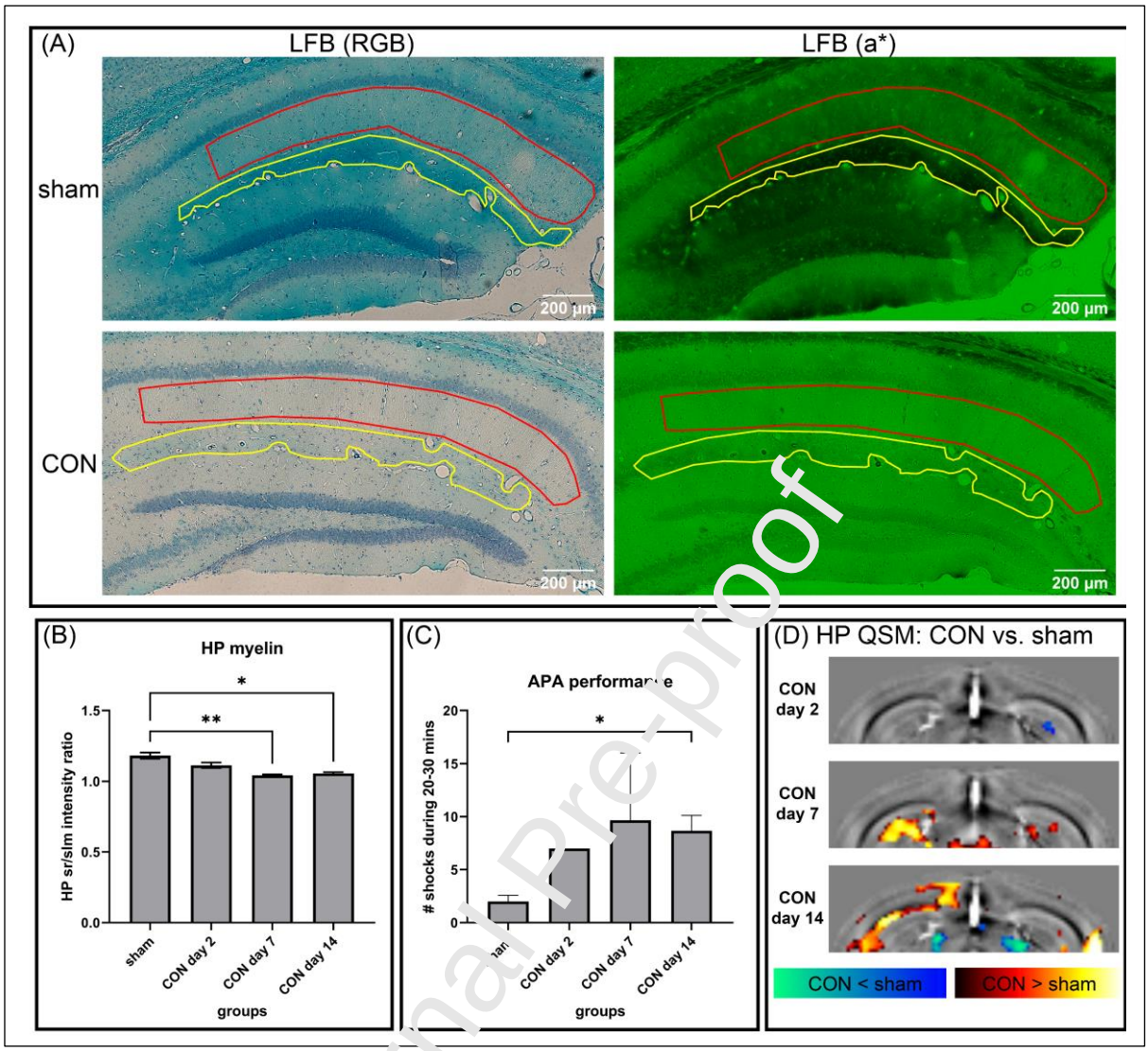

Figure 1. Histology of myelination of the hippocampus and the associated susceptibility and functional imaging.

(A) Examples of quantification of myelination in the lacunosum-moleculare (slm) layer (yellow bounding box). LFB RGB microscopy images were converted to CIELAB colour space L*a*b stack and the LFB (a*) images were chosen for the highest contrast for myelin. Myelination level of the slm layer was quantified by dividing the a* value quantified from the low myelin stratum radiatum (sr) area (red bounding box, light LFB stain, and light appearance on LFB [a*] image) by the a* value quantified from the high myelin slm area (yellow bounding box, darker LFB stain, and dark appearance on LFB [a*] image). Demyelination in TBI animals is indicated when the slm and sr areas have similar LFB staining and low sr/slm intensity ratio.

(B) Stratum lacunosum-moleculare (slm) layer myelination quantified from the LFB intensity ratio by dividing the a* values of the low myelin sr area by that of the high myelin slm area. Lower values indicate less myelination and more demyelination. P

value < 0.05, ** P value < 0.01, uncorrected Dunn's post-hoc test of Kruskal-Wallis one-way ANOVA.

(C) Cumulative number of shocks received by animals in different cohorts during the 20–30 minute interval of the 30-minutes single active placement avoidance (APA) trial. * P < 0.05, uncorrected Dunn's post-hoc test of Kruskal-Wallis one-way ANOVA.

(D) Voxelwise statistical analysis results of quantitative susceptibility mapping (QSM) at CON days 2 (n = 7), 7 (n = 8), and 14 (n = 10) vs. sham (n = 12) in the hippocampal area. Statistical map thresholded at P value < 0.05 (two-tailed), unpaired two samples t-test with a nuisance covariate, implemented as permutation tested for the general linear model, corrected for multiple comparisons with mass-based FSL's threshold-free cluster enhancement (TFCE).

We quantified myelin density of the stratum lacunosum-moleculare (slm) layer of the hippocampus by dividing the a* values of the low myelin stratum radiatum (sr) area (light LFB stain, higher a* value, and "lighter" on a* image) by that of the high myelin slm area (darker LFB stain, lower a* value, and "darker" on a* image) (see Figure 1B for details); a demyelinated slm layer would have a lower ratio. Similarly, myelin density was quantified by dividing the a* value of low myelin tissue by that of the highly myelinated WM tracts.

MRI data processing

All MRI data were exported in DICOM format using Paravision 6.0.1, after which data were converted to the NIFTI format using the dcm2nii tool in MRIcron.[31]

QSM reconstruction

Brain masking was performed on the signal inhomogeneity-corrected mGRE-MRI structural representation image using 3D pulsed-couple neural networks (3D PCNN)[32] followed by manual editing. Masked phase data from mGRE-MRI scans were used to reconstruct QSM images via STI Suite (v.3.0).[33] Raw phase data were unwrapped using a Laplacian-based phase unwrapping method.[34] Background phase removal was performed using the V-SHARP method[35] with filter size of 6. The inverse QSM problem was solved from local tissue phase values using the iLSQR method.[33,36] This QSM pipeline has been demonstrated to be robust.[37] Given the previously reported temporal dependence of QSM,[38] instead of using all echo QSM, only echo images corresponding to echoes 4 to 7 (TEs =

12.395 – 22.136 ms) were averaged to improve image quality. This led to a new averaged QSM image across 4 TEs for analysis.

Six datasets were excluded from the final analysis due to excessive motion artefacts on the reconstructed QSM images, such that final numbers of animals in each cohort were: Sham (n = 12; days 2 (n = 5), 7 (n = 3) and 14 (n = 4) day 14), CON days 2 (n = 7), 7 (n = 8), and 14 (n = 10).

Diffusion MRI processing and data fitting

Opposite phase-encoding direction EPI images for the DWI data were used to calculate the warping field required for EPI distortion correction using FSL's TOPUP tool.[39] The obtained warping fields were applied on the DWI data and eddy current and head-movement induced apparent motions were corrected for using FSL's *eddy_correct*. This motion and eddy current corrected data were fitted through the diffusion tensor model using DWI of b-values = 0 and 1500 s/mm^2 by FSL's DTIFIT tool. All b-value shells data were fitted through the neurite orientation dispersion and density imaging (NODDI) model using the NODDI MATLAB Toolbox (https://www.nitrc.org/projects/noddi_toolbox).[40,41] With regards to specific NODDI model parameters, neurites were modelled as impermeable sticks (cylinders with zero radius) in a homogeneous background, neurite orientation distribution were modelled as Watson's distribution, and the tortuosity model of Szafer for randomly packed cylinders was used to estimate hindered diffusivity, free diffusivity, and neurite packing density.[42]

Structural image processing and multi-modal image registration

During image registration, images were given a header file with voxel size 20 times larger than the original voxel size, to match the size of the human brain template.[43] Structural images were co-registered using the procedure described in our earlier publication.[18] The TE = 9.148 ms mGRE-MRI magnitude image was used as a structural representation image for the mGRE-MRI data; the magnitude image at this echo was determined to have the best balance of GM-WM contrast versus signal drop-off in brain-air interface regions. This mGRE-MRI structural representation image was corrected for signal inhomogeneity using the N4ITK bias field correction[44] as implemented in Advanced Normalization Tool (ANTs v.2.3.4).[45] Each subject's signal inhomogeneity-corrected magnitude image was rigidly registered to the corresponding subject's signal inhomogeneity-corrected T2w structural

image, and the resulting transformation matrix was combined with the structural image non-linear warp fields into a unified mGRE-MRI-to-common space warping field. QSM images were Gaussian filtered using an isotropic 0.3 mm^3 kernel; the brain masks and Gaussian filtered images were spatially normalized to the common space using the unified warping fields described above. All subjects' normalized brain masks were used to define a common space brain mask covering voxels overlapping for all subjects.

Diffusion MRI data were registered together using an iterative image registration and template building based on the b0 image as described in our earlier manuscript.[46] Briefly, the processed diffusion data had the b0 images extracted, averaged, and corrected with N4ITK biasfield correction,[44] and the b0 images were used for an iterative image registration and template creation using antsMultivarateTemplateConstruction2.sh. The obtained warping fields were then used to warp the diffusion metrics to a common space.

Statistical analysis

Active Placement Avoidance analysis

The number of entries into the shock zone for each animal during the 30 minutes APA trial was binned into 5-minute intervals, and this data was used for further analysis of each cohort's performance. Statistical analysis of APA performance was done in Prism 9 (GraphPad Software, CA, USA). Comparison across cohorts was performed using repeated measures ANOVA with Geisser–Greenhouse correction, with cohorts and time intervals as the two factors. Post-hoc statistical tests on the number of entries into the shock zone between the TBI cohorts and the sham cohort were conducted and corrected for multiple comparisons using the two-stage linear step-up procedure of the Benjamini, Krieger, and Yekutieli false discovery rate correction.[47] APA performance within each cohort was analysed using the repeated measures one-way ANOVA with Geisser-–Greenhouse correction and post-hoc statistical tests were conducted with uncorrected Fisher's least squared difference test.

Histology analysis

Myelin quantification values were plotted and analysed using Prism 9 (GraphPad Software, CA, USA); group differences were analysed using the Kruskal-Wallis one-way analysis of variance (ANOVA) test and uncorrected Dunn's test comparing each TBI group

against the sham group. Susceptibility values of the WM and slm layer quantified from the subjects selected for histology were plotted and analysed similarly as above, except that the one-way ANOVA step was an ordinary parametric one-way ANOVA.

Two-samples statistical inference of CON cohorts vs. sham cohort

Voxel-wise two-samples t-tests comparing CON day 2 vs. sham, CON day 7 vs. sham, and CON day 14 vs. sham were performed on spatially normalized susceptibility maps and hippocampal functional connectivity maps using permutation inference for the General Linear model[48] as implemented in FSL's randomise;[49] the number of permutation was set to 20,000 or exhaustive, whichever number was smaller. The resulting QSM statistical maps were corrected for multiple comparisons with mass-based FSL's threshold-free cluster enhancement (TFCE) [50] and thresholded at P value < 0.05 (two-tailed). The signal compartment statistical maps were thresholded at voxel-wise P value < 0.05 (two-tailed).

Correlation between QSM and histology or diffusion MRI

Quantified myelin values and susceptibility values quantified from the corresponding regions were correlated using Spearman correlation. Regions of interest (ROIs) were used to quantify susceptibility from the hippocampal area and white matter area (Supplementary data 1). The structural template that served as the common space for mGRE-MRI data was registered to the generated diffusion b0 template and the ROIs in mGRE-MRI template space were transformed to diffusion MRI template space; the ROIs were used to quantify the Fractional Anisotropy (FA), Neurite Density Index (NDI), and Orientation Dispersion Index (ODI) and the correspondence of diffusion metrics and susceptibility values were analysed using Spearman's correlation in Prism 9 (GraphPad Software, CA, USA).

Results

(A)	ANOVA table	SS	DF	MS	F (DFn, DFd)	P value
	time x cohort	84.95	15	5.66	F (15, 95) = 2.116	**P=0.02**
	time	43.75	5	8.75	F (3.415, 64.88) = 3.268	**P=0.02**
	cohort	115.70	3	38.58	F (3, 19) = 1.441	P=0.26
	subjects	508.90	19	26.78	F (19, 95) = 10.00	**P<0.0001**
	Residual	254.30	95	2.68		

(B)	Two-stage linear step-up procedure of Benjamini, Krieger and Yekutieli	Mean difference	Q value
	0-5 interval		
	sham vs. CON day 2	0.8	0.93

sham vs. CON day 7	-0.3	0.93
sham vs. CON day 14	-0.7	0.93
5-10 interval		
sham vs. CON day 2	-0.5	0.87
sham vs. CON day 7	-1.0	0.85
sham vs. CON day 14	-2.6	0.28
10-15 interval		
sham vs. CON day 2	1.4	0.23
sham vs. CON day 7	-1.3	0.34
sham vs. CON day 14	-2.5	**0.02**
15-20 interval		
sham vs. CON day 2	0.3	>0.9999
sham vs. CON day 7	0.0	>0.9999
sham vs. CON day 14	-1.6	0.89
20-25 interval		
sham vs. CON day 2	-2.3	0.15
sham vs. CON day 7	-3.6	**0.09**
sham vs. CON day 14	-4.2	**0.00**
25-30 interval		
sham vs. CON day 2	-3.0	0.13
sham vs. CON day 7	-3.9	0.17
sham vs. CON day 14	-2.5	0.16

Table 1: (A) Two-way repeated measure ANOVA results analysing the the number of shocks received within each of the 5 minute interval during the 30-minute Active Placement Avoidance trial for the sham (n = 7), CON day 2 (n = 5), CON day 7 (n = 5) and CON day 14 (n = 5) cohorts. (B) Post-hoc tests comparing the CON cohorts to the sham cohort at each of the 5-minute test intervals.

APA performance differences

Two-way repeated measures ANOVA analysis showed there was significant effect of cohort (P value = 0.022) and interaction effect of time x cohort (P value = 0.015) on the difference of the number of shock zone entries (Table 1, Figure 2). Post-hoc testing showed that during the 10–15 minute interval, sham animals made fewer entries into the shock zone than CON day 14 animals (Q value = 0.019) and that CON day 2 animals made fewer entries than CON day 14 animals (Q value – 0.015). During the 20–25 minutes interval, sham animals also made fewer entries into the shock zone than CON day 14 animals (Figure 1C).

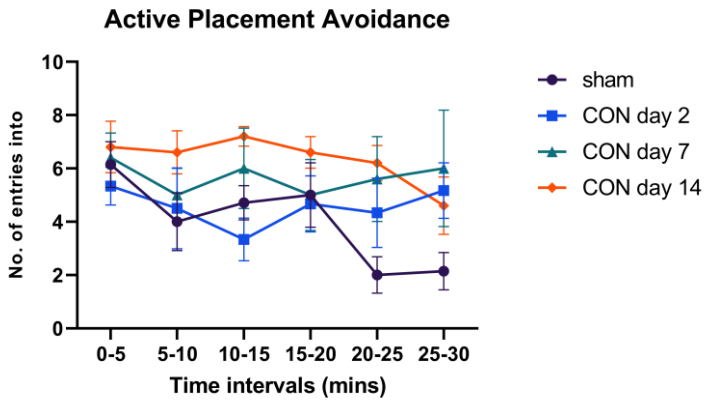

Figure 2: Number of shocks received by animals in the sham (n = 7), CON day 2 (n = 5), CON day 7 (n = 5) and CON day 14 (n = 5) cohorts at each of the 5-minute intervals of a 30-minute single Active Placement Avoidance trial. Data are plotted as mean and standard error of the mean.

Demyelination of the stratum lacunosum-moleculare (slm) layer of the hippocampus

Relative quantification of myelin density in the slm layer showed CON day 7 and CON day 14 groups had significant a lower sr to slm ratio compared the sham group (Dunn's test, P value < 0.05, Figure 1B), indicating that these groups had demyelination in the slm layer of the hippocampus compared. At CON days 7 and 14, QSM detected significantly increased susceptibility in the hippocampal area, with relatively lower susceptibility in the surrounding tissue, indicating that this MRI layer corresponds to the myelin-rich slm layer of the hippocampus (Figure 1D).

Absence of evidence for demyelination of the major white matter tracts

LFB staining showed no discernible difference in myelin staining in the CON group of the major WM tracts, namely the corpus callosum and the fimbriae (Figure 3 and 4A). Similarly, QSM detected no significant difference in the susceptibility of the major WM tracts in CON groups at any timepoint compared to the sham group (Figure 4B).

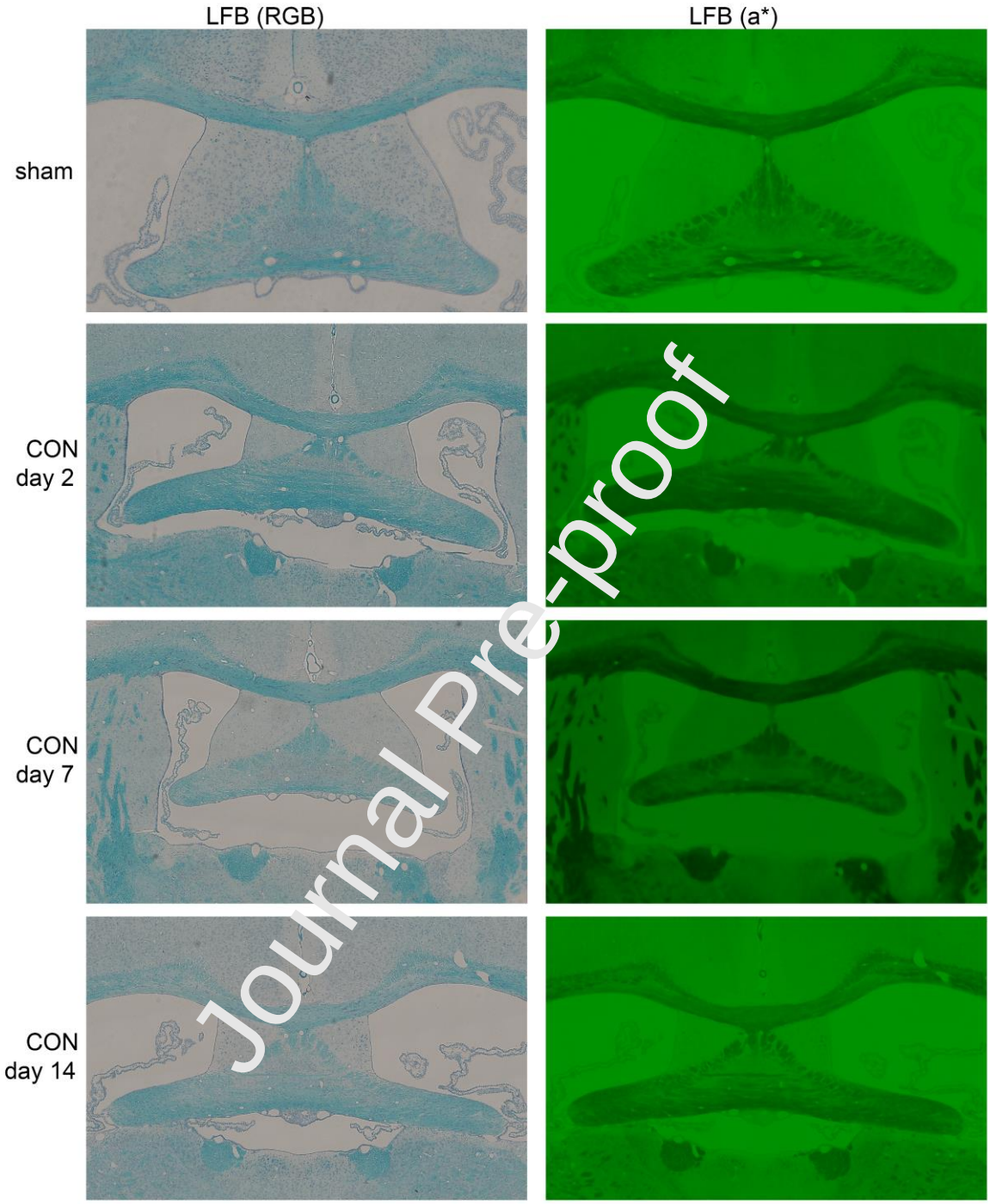

Figure 3. Examples of LFB staining of the major WM tracts, namely the corpus callosum and the fimbriae, and the corresponding a* image of the CIELAB L*a*b stack conversion of the light microscopy LFB staining image.

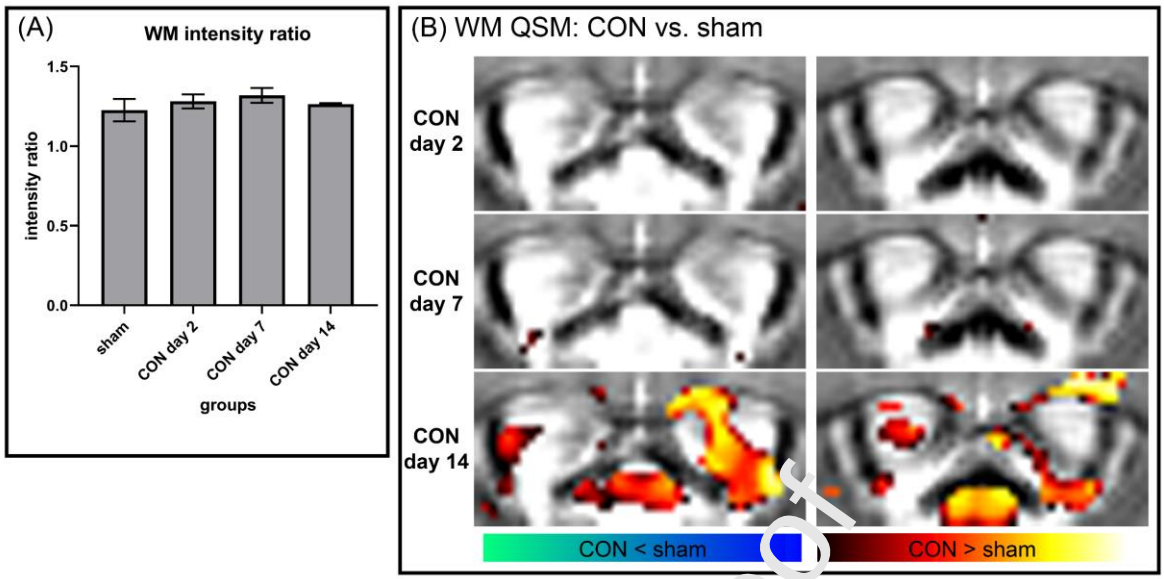

Figure 4. Myelination quantification and susceptibility imaging of the WM tracts in the mouse concussion model

(A) Stratum lacunosum-moleculare (slm) layer myelination was quantified from the LFB intensity ratio by dividing the a* values of the low myelin stratum radiatum (sr) area by that of the high myelin slm area. Lower values indicated less myelination and more demyelination. P value < 0.05, ** P value < 0.01, uncorrected Dunn's post-hoc test of Kruskal-Wallis one-way ANOVA.

(B) Voxel-by-voxel statistical analysis results of quantitative susceptibility mapping (QSM) and CON day 2 (n = 7), CON day 7 (n = 8), and CON day 14 (n = 10) vs. sham (n = 12) in the major white matter tracts areas. Statistical map thresholded at P value < 0.05 (two-tailed), unpaired two samples t-test with a nuisance covariate, implemented as permutation tested for the General Linear Model, corrected for multiple comparisons with mass-based FSL's Threshold-free Cluster enhancement (TFCE).

Correlation of susceptibility measurements with histology or diffusion measurements

Correlation between susceptibility and myelin quantification showed that there was no significant correlation between susceptibility and myelin quantification in the hippocampus (r = 0.35, P value = 0.286) or the white matter areas (r = -0.464, P value = 0.155). Correlation analysis of susceptibility and diffusion MRI metrics (FA, NDI, and ODI) also showed no significant correlation (Figure 5).

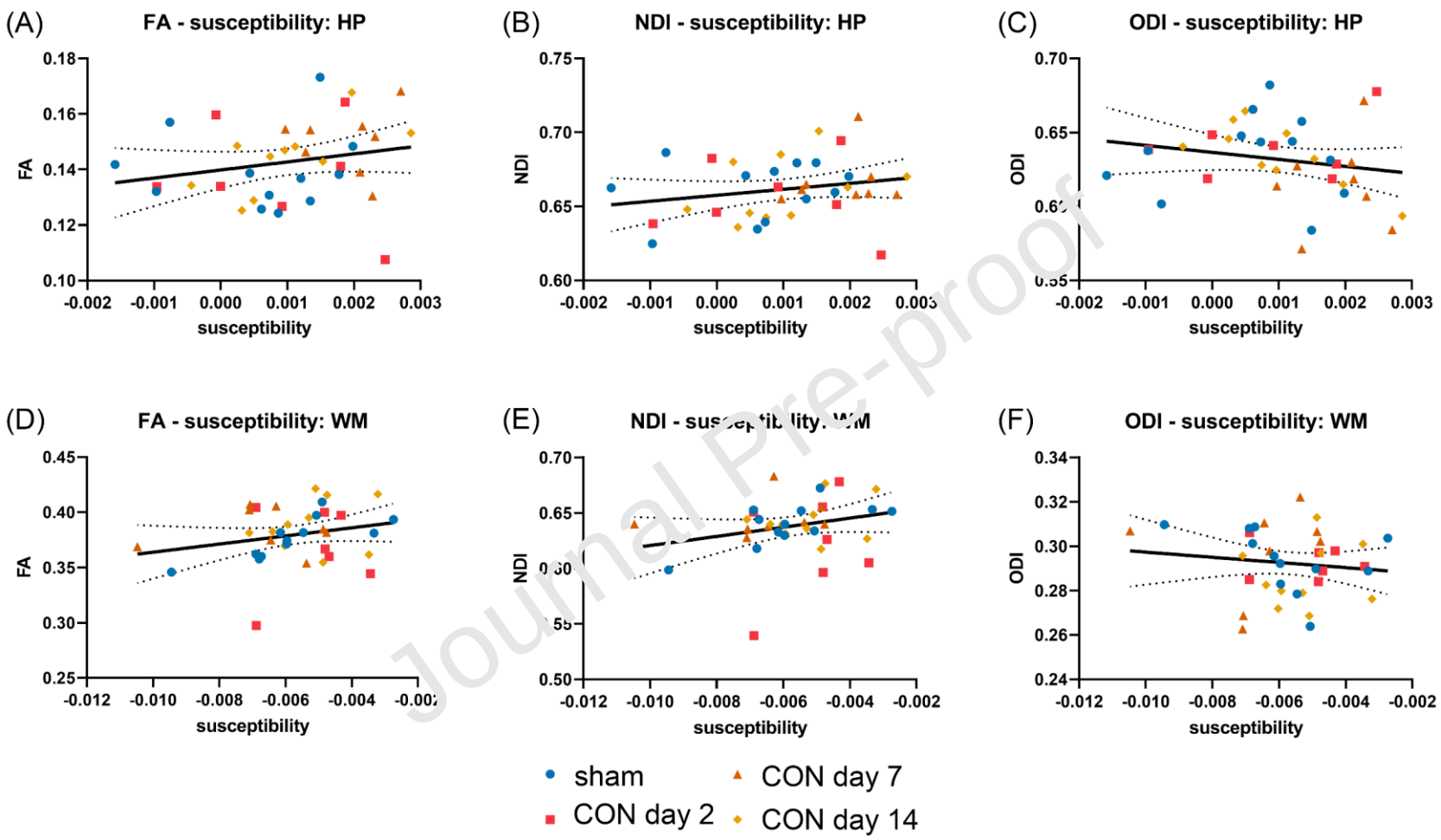

Figure 5: Correlation between DTI and NODDI metrics: Fractional Anisotropy (FA: A, D), Neurite Dispersion Index (NDI: B, E), or Orientation Dispersion Index (ODI: C, F) against susceptibility values quantified from the hippocampal (HP: A – C) and the white matter (WM: D – F) regions of interest. Solid and dotted lines represent the mean and 95% confidence intervals of the linear regression lines.

Discussion

Here we provided preliminary evidence that mice subjected to concussive injury showed demyelination evident on histological analysis of hippocampus and increased susceptibility on QSM scans, which was associated with poorer performance on a measure of spatial memory. These results suggest that subtly altered WM integrity in hippocampal projections manifest in behavioral deficits in our concussion model.

Hippocampal-related spatial learning deficits and axonal injury in concussion

The hippocampus is particularly vulnerable to moderate-to-severe TBI in humans, with demonstrable neuronal degeneration.[51–53] The hippocampus also has drawn widespread attention due to its selective vulnerability and changes in excitability after perturbations and injury in rodent models of TBI.[54–59] Previous work showed that demyelination in the hippocampus and spatial learning impairments peaked between 1 and 2 weeks after blast-induced mild TBI.[60] In a male rat drop-weight model of mTBI, hippocampal long-term potentiation were significantly reduced at 7 day post-injury, but gradually normalized at later timepoints.[61] Others showed that repetitive piston-driven closed-head injuries resulted in significant spatial learning deficits, axonal damage, and microglial reactivity in the hippocampus, in addition to other WM tracts.[62] In this work, LFB staining confirmed the occurrence of demyelination in the slm layer of the hippocampus, which plausibly contributes to the spatial learning deficits seen between 7 and 14 days post-injury; the slm is a relay between the entorhinal cortex and the CA1 of the hippocampus.[63] These findings are consistent with the temporal and spatial patterns of WM changes in other rodent TBI studies discussed above. The same slm area showed increased susceptibility on QSM in the concussion animals, which has been previously associated with demyelination.[23] On the other hand, QSM did not detect significant changes in the major WM tracts of the concussion groups, a finding which was also confirmed by LFB staining. This demonstrates a particular vulnerability of the hippocampal neurites for demyelination injury in this concussion model corresponding to a mild TBI. This result refines the abundance of evidence that hippocampus is particularly vulnerable in human TBI[51–53] and in animal models.[54–59]

Neuroimaging findings in concussion

Human QSM concussion studies have reported unchanged,[64–66] and increased susceptibility in WM post-injury.[67,68] Increased susceptibility in WM tracts of concussed

athletes, which could be attributable to demyelination and/or oedema; the increase peaked at approximately 8 days post-injury.[67] Our imaging and histological staining support the proposition that QSM reveals demyelination only in the myelin-rich layer of the hippocampus, not necessarily extending to the major WM tracts, indicating the higher relative sensitivity of the slm region [53,59] towards traumatic demyelination. This structure is a key substrate in the communication between the entorhinal cortex and the CA1 of the hippocampus, such that its demyelination could contribute to spatial learning deficits. Our earlier diffusion MRI results in the same model showed no diffusion MRI metric changes in the hippocampus.[18] The present QSM results showing increased susceptibility are consistent with susceptibility changes tracking histologically confirmed demyelination[23], and the spatial patterns of increased susceptibility match the patterns of demyelination and axonal damage post-mTBI in rodent models. [60,62] The accord between results indicates that QSM may furnish better sensitivity and specificity for the detection of axonal damage in the hippocampal area following mild TBI.

Other human studies reported no susceptibility changes, with[66] or without diffusion MRI changes[64,65] (Wright et al. reported reduced myelin water fraction[65]) and increased susceptibility in WM and a positive correlation between susceptibility changes and the time off required prior to return to play.[67] On the other hand, decreased susceptibility in human cortical GM was also associated with worse post-concussion symptoms.[68] QSM has also been demonstrated to detect post-concussion changes in the cerebral venous oxygen saturation, which can be relatively easily measured from major cerebral veins. [69,70] This further strengthen the case for the utility of QSM for detecting functionally relevant brain changes that are inconspicuous to conventional imaging procedures.

Limited correlation of QSM and histology or diffusion imaging

The results in this study showed that quantified susceptibility, even from ROIs that showed significant difference between groups and had significant confirmed difference in LFB, had limited correlation with quantified myelin levels. Furthermore, susceptibility values and diffusion metrics (FA, ODI, and NDI) quantified from the same ROIs also did not correlate. This can represent a limitation for neuroimaging modalities whereas controlled and isolated experimental manipulations, for example, cuprizone treatment to induce demyelination,[23] may demonstrate a specific correlation between underlying biological phenomena and neuroimaging measures, for example, increased susceptibility reflecting

demyelination,[23] their performance can be limited in complex real world pathologies. This limitation may be especially noticeable when in milder severities as compared to more severe ones: both diffusion MRI and QSM demonstrated significant findings and correlations in another mouse model of moderate-severe TBI where tissue losses and injuries were readily visible.[71] Nevertheless, neuroimaging methods can still have functional and working values in these conditions, e.g., diffusion MRI being able to differentiate varying injury severities even within the mild classification,[19] or diffusion MRI metrics correlated with an index of anxiety-related behaviors post-TBI.[18] The results of this study showed that while QSM and demyelination quantification did not correlated on an individual basis, QSM comparing TBI and control groups showed significant changes at post-TBI timepoints where significant demyelination were found on histology.

Limitations

We note certain limitations of our study. We did not perform histological analysis in all samples. We note that the LFB histology may have captured only the more severe demyelination, without having sufficient sensitivity to more subtle and varied axonal injuries, especially in the major WM tracts. The study exclusively used male animals. Currently, there is an ongoing debate about how sex may influence the outcome of traumatic brain injury (TBI), ,[72] which may potentially be related to differences in sex and hormones. The decision to use only male animals were made to limit one potential confounding factor and to have methodological consistency with the earlier manuscripts that the injury model used in this study was based on.[73,74]

Conclusion

This work is the first to combine evidence from a histological marker of demyelination, QSM neuroimaging, and spatial learning deficit in a mouse model of concussion, thus providing an integrated view of the biological underpinnings of brain dysfunction following concussion. The results also highlights the potential of QSM as an MRI modality with sensitivity and specificity for detection of hippocampal demyelination. Increased susceptibility was confirmed to be associated with demyelination in a myelin-rich area of the hippocampus in this mouse model of concussion. Present results provide a platform for conducting larger interventional studies aimed at improving outcome following concussion.

Data availability statement

Data from this study is available, without reservations, on request to the corresponding author.

Ethical statements

The authors certify that the animal experiments described in the manuscript was conducted in compliance with the relevant Australian state and federal guidelines legislations, including The Australian Code for the Care and Use of Animals for Scientific Purposes (8th Edition, updated 2021) and The Animal Care and Protection Act (2001). The Australian code for the care and use of animals for scientific purposes is in line with the ARRIVE guidelines and with the U.K. Animals (Scientific Procedures) Act, 1986.

The authors certify that all animal experiments were approved by the Institutional Animal Ethics Committee at the University of Queensland (Animal Ethics Committee approval number QBI/260/17).

Role of funding source

This research was supported by Motor Accident Insurance Commission (MAIC), The Queensland Government, Australia (grant number: 2014000857) and The University of Queensland (Promoting Women's fellowship: CRM 200221-005374). The funders play no role in the study design; the collection, analysis, and interpretation of data, the writing of and decision to submit this manuscript.

Acknowledgement

We acknowledge the support from the Queensland NMR Network and the National Imaging Facility (a National Collaborative Research Infrastructure Strategy capability) for the operation of 9.4T MRI and utilization of image processing computational resources at the Centre for Advanced Imaging, the University of Queensland. We also acknowledge the support and assistance from Dr. Robert Sullivan and the Queensland Brain Institute's Histology Facility for the histological experiments. We acknowledge the support and assistance from Dr. Arnaud Gaudin and the Queensland Brain Institute's Advanced Microscopy Facility for the microscopy imaging using the Axio Imagers and ZEISS ZEN software.

Conflict of interest declaration

All authors hereby declare no competing interest.

Supplementary materials

Supplementary material 1: (Top row) Regions of interest (ROIs) used to quantify susceptibility from the hippocampal area (red) and white matter area (blue) overlaid on the susceptibility map averaged across all subjects' registered data. (Bottom row) susceptibility map averaged across all subjects' registered data without the ROI overlays.

Supplementary material 2: 4D NIFTI image of fitted and registered susceptibility maps of all subjects used in the analysis, stacked in the time dimension. Volumes (starts from 0) 0 – 6: CON day 2, 7 – 14: CON day 7, 15 – 24: CON day 14, 25 – 37: sham. This material is available on the University of Queensland Research Data Management system at this DOI: https://doi.org/10.48610/98780e7

References

1. Cassidy JD, Carroll L, Peloso P, et al. Incidence, risk factors and prevention of mild traumatic brain injury: results of the who collaborating centre task force on mild traumatic brain injury. *J Rehabil Med*. 2004;36(SUPPL. 43):28-60. doi:10.1080/16501960410023732
2. Capruso DX, Levin HS. Cognitive impairment following closed head injury. *Neurol Clin*. 1992;10(4):879-893.
3. Ryan LM, Warden DL. Post concussion syndrome. *Int Rev Psychiatry*. 2003;15(4):310-316. doi:10.1080/09540260310001606692
4. Monti JM, Voss MW, Pence A, McAuley E, Kramer AF, Cohen NJ. History of mild traumatic brain injury is associated with deficits in relational memory, reduced hippocampal volume, and less neural activity later in life. *Front Aging Neurosci*. 2013;5(AUG):1-9. doi:10.3389/fnagi.2013.00041
5. Williamson IJS, Goodman D. Converging evidence for the under-reporting of concussions in youth ice hockey. *Br J Sports Med*. 2006;40(2):128-132. doi:10.1136/bjsm.2005.021832
6. Meehan WP, Mannix RC, Oêbrien MJ, Collins MW. The prevalence of undiagnosed concussions in athletes. *Clin J Sport Med*. 2013;23(5):339-342. doi:10.1097/JSM.0b013e318291d3b3
7. McCrea M, Meier T, Huber D, et al. Role of advanced neuroimaging, fluid biomarkers and genetic testing in the assessment of sport-related concussion: A systematic review. *Br J Sports Med*. 2017;51(12):919-929. doi:10.1136/bjsports-2016-097447
8. Miles L, Grossman RI, Johnson G, Babb JS, Diller L, Inglese M. Short-term DTI predictors of cognitive dysfunction in mild traumatic brain injury. *Brain Inj*.

2008;22(2):115-122. doi:10.1080/02699050801888816

9. Aoki Y, Inokuchi R, Gunshin M, Yahagi N, Suwa H. Diffusion tensor imaging studies of mild traumatic brain injury: a meta-analysis. *J Neurol Neurosurg Psychiatry*. 2012;83(9):870-876. doi:10.1136/jnnp-2012-302742
10. Brandstack N, Kurki T, Tenovuo O. Quantitative diffusion-tensor tractography of long association tracts in patients with traumatic brain injury without associated findings at routine MR imaging. *Radiology*. 2013;267(1):231-239. doi:10.1148/radiol.12112570
11. Yuh EL, Cooper SR, Mukherjee P, et al. Diffusion Tensor Imaging for outcome prediction in mild traumatic brain Injury: a TRACK-TBI study. *J Neurotrauma*. 2014;31(17):1457-1477. doi:10.1089/neu.2013.3171
12. Bazarian JJ, Zhong J, Blyth B, Zhu T, Kavcic V, Peterson D. Diffusion Tensor Imaging detects clinically important axonal damage after mild Traumatic Brain Injury: a pilot study. *J Neurotrauma*. 2007;24(9):1447-1459. doi:10.1089/neu.2007.0241
13. Mayer AR, Ling J, Mannell M V., et al. A prospective diffusion tensor imaging study in mild traumatic brain injury. *Neurology*. 2010;74(8):643-650. doi:10.1212/WNL.0b013e3181d0ccdd
14. Ling JM, Peña A, Yeo RA, et al. Biomarkers of increased diffusion anisotropy in semi-acute mild traumatic brain injury: A longitudinal perspective. *Brain*. 2012;135(4):1281-1292. doi:10.1093/brain/aws073
15. Eierud C, Craddock RC, Fletcher S, et al. Neuroimaging after mild traumatic brain injury: Review and meta-analysis. *NeuroImage Clin*. 2014;4:283-294. doi:10.1016/j.nicl.2013.12.009
16. Wortman RC, Mecum A, Neale KJ, et al. Diffusion MRI abnormalities in adolescent rats given repeated mild traumatic brain injury. *Ann Clin Transl Neurol*. 2018;5(12):1588-1598. doi:10.1002/acn3.667
17. Haber M, Hutchinson EB, Sadeghi N, et al. Defining an analytic framework to evaluate quantitative MRI markers of traumatic axonal njury: Preliminary Results in a Mouse Closed Head Injury Model. *eNeuro*. 2017;4(5):ENEURO.0164-17.2017. doi:10.1523/ENEURO.0164-17.2017
18. To XV, Nasrallah FA. A roadmap of brain recovery in a mouse model of concussion: insights from neuroimaging. *Acta Neuropathol Commun*. 2021;9(1):2. doi:10.1186/s40478-020-01098-y
19. To XV, Benetatos J, Soni N, et al. Ultra-High-Field Diffusion Tensor Imaging Identifies Discrete Patterns of Concussive Injury in the Rodent Brain. *J Neurotrauma*.

2021;38(8):967-982. doi:10.1089/neu.2019.6944

20. Wang Y, Liu T. Quantitative Susceptibility Mapping (QSM): Decoding MRI data for a tissue magnetic biomarker. *Magn Reson Med*. 2015;73:82-101. doi:10.1002/mrm.25358
21. Zhang Y, Gauthier SA, Gupta A, et al. Quantitative Susceptibility Mapping and R2* Measured Changes during White Matter Lesion Development in Multiple Sclerosis: Myelin Breakdown, Myelin Debris Degradation and Removal, and Iron Accumulation. *Am J Neuroradiol*. 2016;37(9):1629-1635. doi:10.3174/ajnr.A4825
22. Ziser L, Meyer-Schell N, Kurniawan ND, et al. Utility of gradient recalled echo magnetic resonance imaging for the study of myelination in cuprizone mice treated with fingolimod. *NMR Biomed*. 2018;31(3):1-13. doi:10.1002/nbm.3877
23. Wang N, Zhuang J, Wei H, Dibb R, Qi Y, Liu C. Probing demyelination and remyelination of the cuprizone mouse model using multimodality MRI. *J Magn Reson Imaging*. 2019;50(6):1852-1865. doi:10.1002/jmri.26758
24. Schweser F, Kyyriäinen J, Preda M, et al. Visualization of thalamic calcium influx with quantitative susceptibility mapping as a potential imaging biomarker for repeated mild traumatic brain injury. *Neuroimage*. 2019;200(1):250-258. doi:10.1016/j.neuroimage.2019.06.024
25. Willis EF, Bartlett PF, Vukovic J. Protocol for short- and longer-term spatial learning and memory in Mice. *Front Behav Neurosci*. 2017;11(October). doi:10.3389/fnbeh.2017.00197
26. Nasrallah FA, To XV, Chen D, Routtenberg A, Chuang K. Functional connectivity MRI tracks memory networks after maze learning in rodents. *Neuroimage*. 2016;127:196-202. doi:10.1016/j.neuroimage.2015.08.013
27. Churchill NW, Caverzasi E, Graham SJ, Hutchison MG, Schweizer TA. White matter microstructure in athletes with a history of concussion: Comparing diffusion tensor imaging (DTI) and neurite orientation dispersion and density imaging (NODDI). *Hum Brain Mapp*. 2017;38(8):4201-4211. doi:10.1002/hbm.23658
28. Nasrallah FA, Tay H, Chuang K. Detection of functional connectivity in the resting mouse brain. *Neuroimage*. 2014;86:417-424. doi:10.1016/j.neuroimage.2013.10.025
29. Schindelin J, Arganda-Carreras I, Frise E, et al. Fiji: an open-source platform for biological-image analysis. *Nat Methods*. 2012;9(7):676-682. doi:10.1038/nmeth.2019
30. Schwiegerling J. *Field Guide to Visual and Ophthalmic Optics*. SPIE Press; 2004.
31. Rorden C, Brett M. Stereotaxic display of brain lesions. *Behav Neurol*.

2000;12(4):191-200. doi:10.1155/2000/421719

32. Chou N, Wu J, Bai Bingren J, Qiu A, Chuang K-H. Robust automatic rodent brain extraction using 3-D pulse-coupled neural networks (PCNN). *IEEE Trans Image Process*. 2011;20(9):2554-2564. doi:10.1109/TIP.2011.2126587
33. Li W, Wang N, Yu F, et al. A method for estimating and removing streaking artifacts in quantitative susceptibility mapping. *Neuroimage*. 2015;108(10):111-122. doi:10.1016/j.neuroimage.2014.12.043
34. Li W, Wu B, Liu C. Quantitative susceptibility mapping of human brain reflects spatial variation in tissue composition. *Neuroimage*. 2011;55(4):1645-1656. doi:10.1016/j.neuroimage.2010.11.088
35. Schweser F, Deistung A, Lehr BW, Reichenbach JR. Quantitative imaging of intrinsic magnetic tissue properties using MRI signal phase. An approach to in vivo brain iron metabolism? *Neuroimage*. 2011;54(4):2789-2807. doi:10.1016/j.neuroimage.2010.10.070
36. Wang N, Cofer G, Anderson RJ, Qi Y, Liu C, Johnson GA. Accelerating quantitative susceptibility imaging acquisition using compressed sensing. *Phys Med Biol*. 2018;63(24). doi:10.1088/1361-6560/aaf15d
37. Schweser F, Robinson SD, de Rochefort L, Li W, Bredies K. An illustrated comparison of processing methods for phase MRI and QSM: removal of background field contributions from sources outside the region of interest. *NMR Biomed*. 2017;30(4). doi:10.1002/nbm.3604
38. Sood S, Urriola J, Deutens D, et al. Echo time-dependent quantitative susceptibility mapping contains information on tissue properties. *Magn Reson Med*. 2017;77(5):1946-1958. doi:10.1002/mrm.26281
39. Andersson JLR, Skare S, Ashburner J. How to correct susceptibility distortions in spin-echo echo-planar images: Application to diffusion tensor imaging. *Neuroimage*. 2003;20(2):870-888. doi:10.1016/S1053-8119(03)00336-7
40. Zhang H, Schneider T, Wheeler-Kingshott CA, Alexander DC. NODDI: Practical in vivo neurite orientation dispersion and density imaging of the human brain. *Neuroimage*. 2012;61(4):1000-1016. doi:10.1016/j.neuroimage.2012.03.072
41. Tariq M, Schneider T, Alexander DC, Gandini Wheeler-Kingshott CA, Zhang H. Bingham-NODDI: Mapping anisotropic orientation dispersion of neurites using diffusion MRI. *Neuroimage*. 2016;133:207-223. doi:10.1016/j.neuroimage.2016.01.046

42. Szafer A, Zhong J, Gore JC. Theoretical model for water diffusion in tissues. *Magn Reson Med*. 1995;33(5):697-712. doi:10.1002/mrm.1910330516
43. Bajic D, Craig MM, Mongerson CRL, Borsook D, Becerra L. Identifying rodent resting-state brain networks with independent component analysis. *Front Neurosci*. 2017;11(December). doi:10.3389/fnins.2017.00685
44. Tustison NJ, Avants BB, Cook PA, et al. N4ITK: Improved N3 Bias Correction. *IEEE Trans Med Imaging*. 2010;29(6):1310-1320. doi:10.1109/TMI.2010.2046908
45. Avants BB, Tustison NJ, Stauffer M, Song G, Wu B, Gee JC. The Insight ToolKit image registration framework. *Front Neuroinform*. 2014;8(APR):1-13. doi:10.3389/fninf.2014.00044
46. To XV, Nasrallah FA. Multi-modal magnetic resonance imaging in a mouse model of concussion. *Sci Data*. 2021;8(1):1-13. doi:10.1038/s41597-021-00985-w
47. Benjamini Y, Krieger AM, Yekutieli D. Adaptive linear step-up procedures that control the false discovery rate. *Biometrika*. 2006;93(3):491-507. doi:10.1093/biomet/93.3.491
48. Anderson MJ, Robinson J. Permutation Tests for Linear Models. *Aust N Z J Stat*. 2001;43(1):75-88. doi:10.1111/1467-842X.00156
49. Winkler AM, Ridgway GR, Webster MA, Smith SM, Nichols TE. Permutation inference for the general linear model. *Neuroimage*. 2014;92:381-397. doi:10.1016/j.neuroimage.2014.01.060
50. Smith SM, Nichols TE. Threshold-free cluster enhancement: Addressing problems of smoothing, threshold dependence and localisation in cluster inference. *Neuroimage*. 2009;44(1):83-98. doi:10.1016/j.neuroimage.2008.03.061
51. Kotapka MJ, Graham DI, Adams JH, Gennarelli TA. Hippocampal pathology in fatal non-missile human head injury. *Acta Neuropathol*. 1992;83(5):530-534. doi:10.1007/BF00310031
52. Maxwell WL, Dhillon K, Harper L, et al. There is differential loss of pyramidal cells from the human hippocampus with survival after blunt head injury. *J Neuropathol Exp Neurol*. 2003;62(3):272-279. doi:10.1093/jnen/62.3.272
53. Frankowski JC, Kim YJ, Hunt RF. Selective vulnerability of hippocampal interneurons to graded traumatic brain injury. *Neurobiol Dis*. 2019;129:208-216. doi:10.1016/j.nbd.2018.07.022
54. Gibson KL, Remson L, Smith A, Satterlee N, Strain GM, Daniloff JK. Comparison of nerve regeneration through different types of neural prostheses. *Microsurgery*.

1991;12(2):80-85. doi:10.1002/micr.1920120205

55. Hicks RR, Smith DH, Lowenstein DH, Marie R Saint, Mcintosh TK. Mild Experimental Brain Injury in the Rat Induces Cognitive Deficits Associated with Regional Neuronal Loss in the Hippocampus. *J Neurotrauma*. 1993;10(4):405-414. doi:10.1089/neu.1993.10.405
56. Christidi F, Bigler ED, McCauley SR, et al. Diffusion tensor imaging of the perforant pathway zone and its relation to memory function in patients with severe traumatic brain injury. *J Neurotrauma*. 2011;28(5):711-725. doi:10.1089/neu.2010.1644
57. Bigler ED, Blatter DD, Anderson C V., et al. Hippocampal volume in normal aging and traumatic brain injury. *Am J Neuroradiol*. 1997;18(1):11-28.
58. Lowenstein DH, Thomas MJ, Smith DH, McIntosh TK. Selective vulnerability of dentate hilar neurons following traumatic brain injury. A potential mechanistic link between head trauma and disorders of the hippocampus. *J Neurosci*. 1992;12(12):4846-4853. doi:10.1523/jneurosci.12-12-04846.1992
59. Schumm SN, Gabrieli D, Meaney DF. Plasticity impairment exposes CA3 vulnerability in a hippocampal network model of mild traumatic brain injury. *Hippocampus*. 2022;32(3):231-251. doi:10.1002/hipo.23402
60. Nonaka M, Taylor WW, Bukalo O, et al. Behavioral and Myelin-Related Abnormalities after Blast-Induced Mild Traumatic Brain Injury in Mice. *J Neurotrauma*. 2021;38(11):1551-1571. doi:10.1089/neu.2020.7254
61. White ER, Pinar C, Bostrom CA, Meconi A, Christie BR. Mild Traumatic Brain Injury Produces Long-Lasting Deficits in Synaptic Plasticity in the Female Juvenile Hippocampus. *J Neurotrauma*. 2017;34(5):1111-1123. doi:10.1089/neu.2016.4638
62. Shitaka Y, Tran HT, Bennett RE, et al. Repetitive closed-skull traumatic brain injury in mice causes persistent multifocal axonal injury and microglial reactivity. *J Neuropathol Exp Neurol*. 2011;70(7):551-567. doi:10.1097/NEN.0b013e31821f891f
63. Capogna M. Neurogliaform cells and other interneurons of stratum lacunosum-moleculare gate entorhinal-hippocampal dialogue. *J Physiol*. 2011;589(8):1875-1883. doi:10.1113/jphysiol.2010.201004
64. Weber AM, Pukropski A, Kames C, et al. Pathological insights from quantitative susceptibility mapping and diffusion tensor imaging in ice hockey players pre and post-concussion. *Front Neurol*. 2018;9(AUG):1-8. doi:10.3389/fneur.2018.00575
65. Wright AD, Jarrett M, Vavasour I, et al. Myelin water fraction is transiently reduced after a single mild traumatic brain injury - A prospective cohort study in collegiate

hockey players. *PLoS One*. 2016;11(2):1-16. doi:10.1371/journal.pone.0150215

66. Gong NJ, Kuzminski S, Clark M, et al. Microstructural alterations of cortical and deep gray matter over a season of high school football revealed by diffusion kurtosis imaging. *Neurobiol Dis*. 2018;119(March):79-87. doi:10.1016/j.nbd.2018.07.020
67. Koch KM, Meier TB, Karr R, Nencka AS, Muftuler LT, McCrea M. Quantitative Susceptibility Mapping after Sports-Related Concussion. *Am J Neuroradiol*. 2018;39(7):1215-1221. doi:10.3174/ajnr.A5692
68. Koch KM, Nencka AS, Swearingen B, Bauer A, Meier TB, McCrea M. Acute Post-Concussive Assessments of Brain Tissue Magnetism Using Magnetic Resonance Imaging. *J Neurotrauma*. 2020;10:1-10. doi:10.1089/neu.2020.7322
69. Chai C, Guo R, Zuo C, et al. Decreased susceptibility of major veins in mild traumatic brain injury is correlated with post-concussive symptoms: A quantitative susceptibility mapping study. *NeuroImage Clin*. 2017;15(February):625-632. doi:10.1016/j.nicl.2017.06.008
70. Wright DK, O'Brien TJ, Shultz SR. Sub-acute Changes on MRI Measures of Cerebral Blood Flow and Venous Oxygen Saturation in Concussed Australian Rules Footballers. *Sport Med - Open*. 2022;9(1). doi:10.1186/s40798-022-00435-w
71. Soni N, Vegh V, To XV, Mohamed AZ, Borges K, Nasrallah FA. Combined Diffusion Tensor Imaging and Quantitative Susceptibility Mapping Discern Discrete Facets of White Matter Pathology Post-injury in the Rodent Brain. *Front Neurol*. 2020;11(March):1-16. https://doi.org/10.3389/fneur.2020.00153
72. Gupte R, Brooks W, Vukas R, Pierce J, Harris J. Sex Differences in Traumatic Brain Injury: What We Know and What We Should Know. *J Neurotrauma*. 2019;36(22):3063-3091. doi:10.1089/neu.2018.6171
73. Namjoshi DR, Cheng WH, McInnes KA, et al. Merging pathology with biomechanics using CHIMERA (Closed-Head Impact Model of Engineered Rotational Acceleration): a novel, surgery-free model of traumatic brain injury. *Mol Neurodegener*. 2014;9(55):55. doi:10.1186/1750-1326-9-55
74. Namjoshi DR, Cheng WH, Bashir A, et al. Defining the biomechanical and biological threshold of murine mild traumatic brain injury using CHIMERA (Closed Head Impact Model of Engineered Rotational Acceleration). *Exp Neurol*. 2017;292:80-91. doi:10.1016/j.expneurol.2017.03.003

Conflict of interest declaration

All authors hereby declare no competing interest.

Highlights

- This study combines behaviour, histopathology, and Quantitative Susceptibility Imaging (QSM) to identify the underlying hippocampal changes triggered following concussion.
- Increased susceptibility detected by QSM and demyelination in the hippocampus occurred concurrently post-concussion.
- Spatial learning deficits and demyelination in the hippocampus occurred concurrently post-concussion.